A&A 529, A111 (2011)
DOI: 10.1051/0004-6361/201016244

Astronomy & Astrophysics

A sharp change in the mineralogy of annealed protoplanetary dust at the glass transition temperature

M. Roskosz[1], J. Gillot[1], F. Capet[2], P. Roussel[2], and H. Leroux[1]

[1] Unité Matériaux et transformations, Université Lille1, CNRS, UMR 8207, 59655 Villeneuve d'Ascq, France
e-mail: mathieu.roskosz@univ-lille1.fr
[2] Unité de Catalyse et de Chimie du Solide, ENSCL, Université Lille Nord de France, CNRS, UMR 8181, 59655 Villeneuve d'Ascq, France

Received 1 December 2010 / Accepted 7 March 2011

ABSTRACT

The crystallinity of silicate dust detected in protoplanetary disks contrasts with the dominantly amorphous nature of dust in the interstellar medium. The amorphous-to-crystal transition is therefore a valuable probe to constrain physical properties of disks such as temperature gradients or the extent of radial mixing. However, it requires a comprehensive knowledge of the behaviour of amorphous Mg silicates during thermal processing. In this respect, amorphous analogues of enstatite composition ($MgSiO_3$) were thermally annealed around the glass transition temperature ($T_g \sim 1040$ K). We show that enstatite is not produced below T_g. Instead, the annealing leads to a mineralogical assemblage dominated by forsterite (Mg_2SiO_4). A sharp change is observed at T_g, and pyroxene becomes the dominant mineral species. The annealing conditions marginally change the mineralogical assemblages produced above T_g. A notable exception is the recovery of protoenstatite (the high-temperature polymorph), which appears to be easily quenched in dust analogues. Detection of this phase would then provide an excellent probe for fast thermal events in disks. Our data suggest that below ~1000 K, the mineralogy of silicate dust of solar composition should naturally be dominated by olivine while above this temperature pyroxenes should dominate. They also show that silica polymorphs recently detected in cold regions of disks are the natural by-products of the formation of forsterite out of enstatite precursor. The low-temperature crystallization pathway reported, combined with the evaporation/condensation process, captures the essential features of the zoned mineralogy of protoplanetary disks.

Key words. protoplanetary disks – planets and satellites: formation – planetary nebulae: general

1. Introduction

In the past decade, a large number of experimental studies have been dedicated to the behaviour of dust analogues during annealing to better understand silicate signatures in spectroscopic data acquired from the ground and from orbiters. Despite the large amount of information collected, the nature of cosmic dust (composition and structure from the atomic to the micrometre scale) makes the experimental approach of its transformation more challenging than in traditional experimental mineralogy. This is mainly because of the small grain size of dust and their amorphous structure. The structure and properties of cosmic silicates observed in the interstellar medium and in protoplanetary disks have recently been extensively reviewed (Henning 2010). In both cases, the main dust components are magnesium and iron silicates (Molster et al. 1999; Bouwman et al. 2001; Molster et al. 2002). In the case of interstellar silicates, the iron content is still under debate. A significant fraction of iron is probably sequestered in metallic inclusions or in sulfides (Pollack et al. 1994; Henning & Stognienko 1996; Min et al. 2007). However, direct observational evidence for these grains is lacking so far owing to the absence of a spectral signature (iron has no feature, FeS looses its IR feature rapidly for large grain sizes). Nonetheless, the amount of iron present in the crystal network of the silicate dust must be very low (Henning 2010), as suggested by the fact that *Spitzer* spectra of disks can be modelled by pure enstatite and forsterite (Juhàsz et al. 2010; Watson et al. 2009). It is therefore reasonable to study iron-free analogues. The typical grain size of this dust ranges from a few tens of nanometres to a few microns (Min et al. 2007). Finally, while ISM silicate dust is mainly amorphous, protoplanetary dust appears to be significantly crystallized, which calls for a major processing of the dust during the early evolution of the disk. In this framework, a recurring question still stands concerning how and where this extended phase transformation takes place within the disk. In addition, the detailed structural state of the amorphous silicate dust is not known. Indeed, different formation processes (e.g. direct condensation, melt quench, irradiation) may potentially lead to different amorphous structures, which in turn could result in different crystallization pathways.

As a consequence, a series of Mg-rich analogues were used in the past decade, including condensed smokes and thin films, laser ablation products, glasses and sol-gels (e.g. Hallenbeck & Nuth 1998; Rietmeijer et al. 2002; Brucato et al. 1999; Fabian et al. 2000; Thompson et al. 2003; Jäger et al. 2003; Davoisne et al. 2006). Recently, we showed experimentally that the nature of the minerals formed during the annealing of enstatite amorphous precursor ($MgSiO_3$) depends on temperature (Roskosz et al. 2009). In particular, defining the glass transition temperature as the temperature below which diffusive processes involving the silicate network become extremely slow, we showed that ~60 K below ($T_g \sim 1040$ K determined on synthetic glass), enstatite amorphous precursor did not transform into crystalline enstatite but that instead a significant fraction of forsterite (Mg_2SiO_4) precipitates (Roskosz et al. 2009). Conversely, above this critical temperature, enstatite becomes unambiguously the dominant crystalline mineral. This behaviour was observed for different classes of amorphous material (glasses and sol-gels), which suggests that it may be a general trend independent of the amorphous structure of the starting

Table 1. Experimental conditions and mineralogy of annealed samples.

Temperature (K)	Heating Rate (K/hour)	Run Duration at T (hours)	Mineralogy (relative fractions of the crystalline phases in %)				
			Forsterite	Clinoenstatite	Orthoenstatite	Protoenstatite	Cristobalite
973	300	360	100	–	–	–	–
993	300	240	100	–	–	–	–
1013	300	240	27	14	59	–	–
1033	300	288	22	18.5	57.5	–	–
1176	12 000	15	19	18	63	–	–
1273	7	0	25	27	48	–	–
1273	333	20	25	17	58	–	–
1273	12 000	2	18	19	63	–	–
1378	12 000	15	18	–	–	79	2

Notes. Relative fractions of minerals are determined from XRD patterns. An error of ±5% is typically considered for the method employed (see text).

material. Microscopic controls of this phenomenon were described in terms of mobility decoupling between constituting cations, a mechanism which must be at work in any kind of amorphous silicates (condensates, glasses, irradiation products). However, no temperature-dependence of the relative proportions of the different crystal phases was proposed.

Here we extend the study of Roskosz et al. (2009) of the crystallization of amorphous precursors over a larger temperature range and for different heating conditions. X-ray powder diffraction combined with Raman spectroscopy reveal an unexpected complexity of the transformation behaviour of protoplanetary dust analogues. Our results are discussed in the light of recent *Spitzer* observations and bring more constraints on the mineralogical zoning in disks.

2. Experimental and analytical procedures

2.1. Synthesis of the dust analogue

The $MgSiO_3$ amorphous precursor was prepared by a sol-gel method using TetraEthOxySilane (TEOS) and magnesium nitrates. The conditions were adapted to allow a slow reticulation of the gel and therefore a stoichiometric and homogeneous incorporation of magnesium in the silicate network. Both bulk and microscopic analyses confirmed the homogeneity of the Mg/Si ratio of the gels down to a few hundreds of cubic nanometres. Dehydration, decarbonation and denitrification were performed during slow heating to 773 K in air and recorded by mass spectrometry. Infrared spectroscopy, X-ray diffraction and transmission electron microscopy confirmed the nearly complete dehydration-denitrification, the amorphous structure and the lack of MgO heterogeneities and nanocrystals in the starting materials respectively. The hygroscopic behaviour of these precursors was not a problem in this study because the phase transformations occurred above 973 K and therefore occurred after a slow heating of the material through the dehydration temperature interval.

2.2. Run procedure

Samples were placed in electrical furnaces on a platinum-coated alumina crucible to prevent contamination. We performed isothermal experiments and slow continuous heating to a target temperature. Below 1073 K, the heating rate was 300 K/h, which is fast enough in this temperature range to avoid crystallization during the heating. For the same reason, the heating rate was increased to 200 K/s above 1173 K. The typical temperature

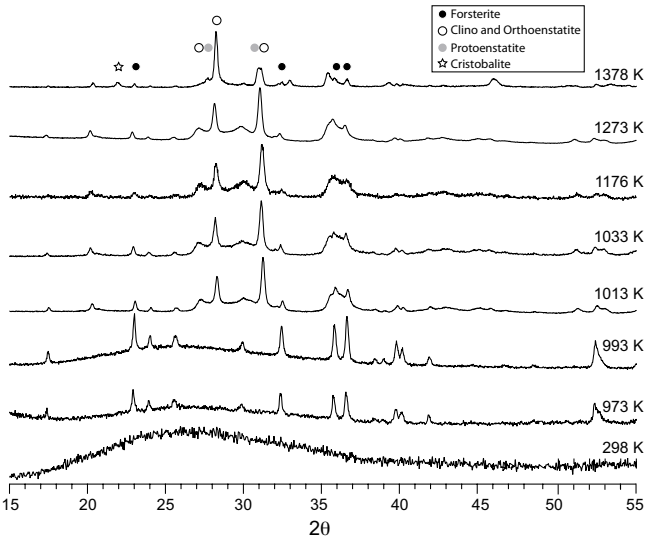

Fig. 1. Powder diffraction patterns of samples annealed at different temperatures (see Table 1). The main characteristic peaks of minerals formed are shown in the top pattern. Below 973 K only forsterite peaks are observed. Above this temperature both ortho- and clinoenstatite form readily. Cristobalite and protoenstatite are recovered in samples quenched from 1378 K only. Indexation of the patterns was done using the software EVA (Bruker-AXS) and the database edited by the International Centre for Diffraction Data (ICDD).

inferred in astrophysical studies for silicate transformation is in the range 600−1000 K. We thus carried out annealing in air from 970 to 1370 K (i.e. starting 60 K below T_g) for up to two weeks (see Table 1). At lower temperature, the crystal growth becomes rapidly too slow to be studied in laboratory. However, the microscopic and physical interpretation of our results make their extrapolation to lower temperatures reliable because studies of amorphous materials down to at least 800 K do not indicate any additional transition in terms of cation mobility (Gruener et al. 2001).

2.3. Analytical methods

A D8 Bruker AXS $\theta-\theta$ diffractometer equipped with a Cu anode was used for room temperature crystal identification by X-ray diffraction in reflexion (Bragg-Brentano geometry). Patterns were recorded for 2θ values ranging from 15 to 85° with a step size of 0.02°. The acquisition time for each step size was fixed to 1.5 s to optimize the signal/noise ratio on partially

crystallized and small samples. Raman spectra were recorded using a HR labRam spectrometer (Horba scientific). The 800 mm focal length system was equipped with a 532 nm laser focused with a 100 X (NA 0.9) objective on the sample. The measured spatial resolution is 0.8 μm. The use of a 1800 g/mm grating permits one to reach a 0.5 cm^{-1} per pixel spectral resolution.

3. Results

Amorphous enstatite precursors ($MgSiO_3$) were annealed at temperatures from 973 to 1378 K. Crystallization was significant even 60 K below T_g (determined at 1040 K on glasses). This result strengthens the kinetic nature of the glass transition. Even below this transition, phase transformation occurs to minimize the free energy of the system. However, here, this crystallisation leads to an unusual mineralogy below T_g. Only forsterite was detected by XRD and Raman spectroscopy (Table 1, Fig. 1). At higher annealing temperatures, orthoenstatite (Oen), clinoenstatite (Cen), protoenstatite (Pen), forsterite (Fo), and cristobalite (Cr, an SiO_2 polymorph) were identified (Table 1, Fig. 1). The XRD patterns were quantified and relative mineral proportions were determined (Table 1). The method employed is less accurate than a Rietveld refinement, which could not be applied here because of the small grain size of the crystallites. The proportion of the remaining amorphous phase cannot be quantified by X-ray diffraction either. As a consequence, the error given on the relative crystalline phase proportions is ±5%. Given this large uncertainty, we note an extremely sharp change in the mineralogy of the annealed samples that takes place between 993 and 1013 K (Fig. 2a). Above 1013 K, the relative proportion of forsterite/enstatite appears to be constant (~20/80). In addition to the abrupt change of mineralogy around T_g, the relative proportions of pyroxene polymorphs continuously varies with temperature (Fig. 2b). This variation reflects the fact that samples are in the stability fields of different polymorphs as temperature increases. In this respect the samples were always quenched as a mixture of Cen or Oen. This is likely due to the metastability of annealing products formed at low temperature or to the sluggish nature of the polymorphic transition Cen-Oen (Smyth 1974). Another high-temperature polymorph of enstatite, protoenstatite, crystallized in the 1378 K experiment. Protoenstatite (Pen), which is unstable below 1273 K and reputedly unquenchable, was recovered without taking specific precautions and was clearly identified by Raman spectroscopy (Fig. 3). The identification of this species is difficult based on XRD patterns because it shares many of the peaks with Cen and Oen. Based on Raman spectra, significant fractions of Cen and Oen must coexist with Pen in this sample. However, by lack of additional robust constraints, XRD pattern can be modelled with 100% of Pen as well as with a mixture of the three polymorphs with at least 50% of Pen.

At 1273 K, the effect of the run duration and heating rates were monitored because reaction rates are sufficiently fast to be studied. One sample was annealed for two hours after a fast heating at 200 K/s to 1273 K. Another was annealed for 20 h after a heating in three hours. A third sample was heated to 973 K at 40 K/h and then up to 1273 K at 7 K/h and finally directly quenched to room temperature. These different procedures do not change the nature of the phases formed and moderately change their relative proportions (Table 1, Fig. 4). Nonetheless, the fraction of forsterite is slightly lower for the sample heated at 200 K/s than for others (18% against 25%) and the fraction of orthoenstatite increases with the heating rate (from 48% to 63%). These results show that only very fast heating of the amorphous precursor can lead to a mineralogical assemblage dominated by the thermodynamically-predicted phase (i.e. orthoenstatite) and limits the formation of forsterite and of metastable clinoenstatite during the heating stage. They also rule out the possibility that low-temperature mineralogical assemblages are only transient intermediate compounds since long and short experiments, slow and fast heating rates essentially lead to the same mineralogy.

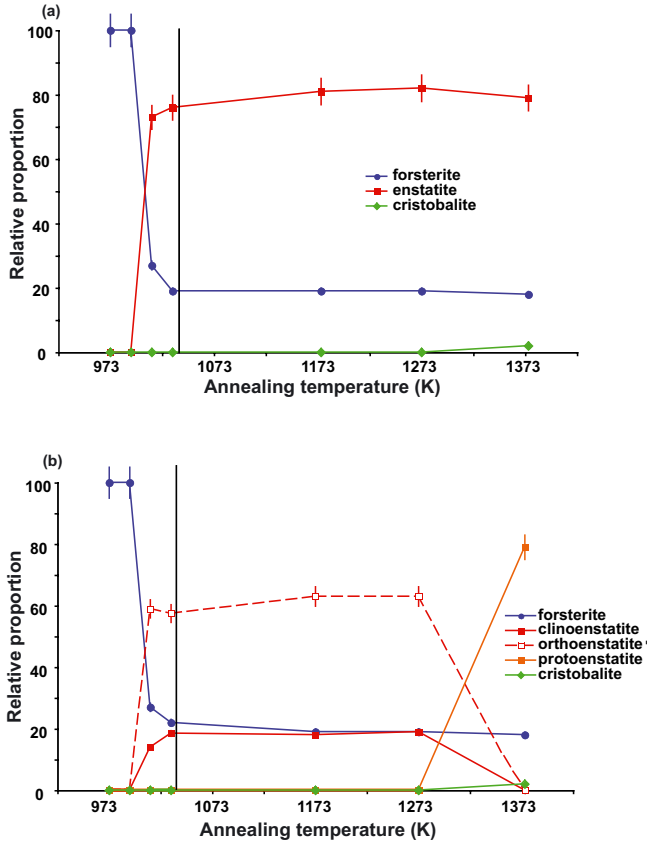

Fig. 2. Relative proportions of the different crystalline phases formed during annealing of the amorphous precursor. These data are derived from XRD patterns (see text for details). In **a)** only the mineralogical family are provided, which gives a direct view of the sharp change of the mineralogy produced as a function of T. In **b)** the different polymorphs of enstatite are presented. The vertical line at 1040 K represents the glass transition temperature determined on quenched glasses.

4. Discussion

4.1. Significance of the sharp mineralogical change to trace thermal events and its microscopic origin

Our experiments show that an abrupt change of mineralogy occurs when amorphous silicate dust is annealed below and above its glass transition temperature. Below T_g, the crystalline silicate formed (forsterite) is the most enriched in alkaline-earth cations (namely magnesium in this study). Above T_g, phases predicted by equilibrium phase diagrams become dominant. This result is generally consistent with results compiled from different works on annealed amorphous materials of enstatite composition (Table 2). This table shows available data as a function of the nature of the amorphous precursor, the peak temperature and the methods of characterization employed. Because the primary goals of these studies were diverse, experimental constraints and analytical methods strongly differ from one study to another. It is therefore particularly striking that the preferential crystallization

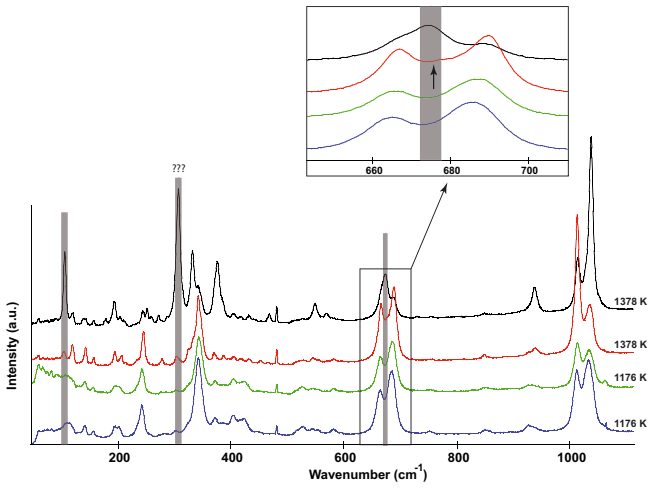

Fig. 3. Typical Raman spectra of samples annealed at 1176 K and 1378 K. The latter temperature is in the stability field of protoenstatite, which is easily quenched for small samples such as dust analogues. For each sample, several spectra were recorded to check the reproducibility of the signature and to make sure that it does not depend on crystal orientation. Here, two characteristic spectra are reproduced for each temperature. The two main regions that significantly differ from other polymorphs are indicated in grey (105 cm^{-1} and 673 cm^{-1}). Note that peak intensities are not considered because they depend on the orientation of the analysed crystals. Yet a third region of interest is indicated in grey (307 cm^{-1}). It may correspond to a band that has a strong intensity in protoenstatite and weak intensities in other polymorphs. The inset shows that the symmetric Si-O-Si bending doublet at 663−685 cm^{-1} in clinoenstatite and orthoenstatite is reduced to a single peak at 673 cm^{-1} in protoenstatite as detailed in Reynard et al. (2008).

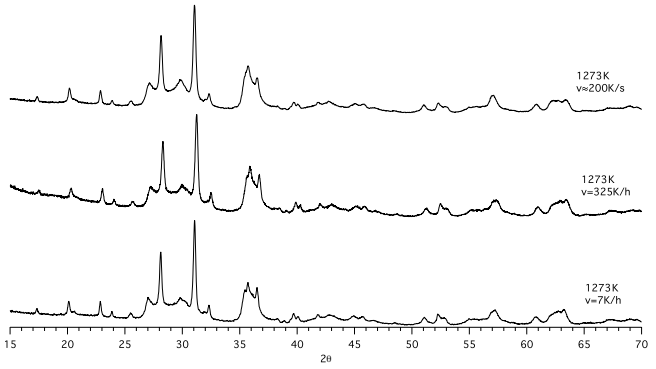

Fig. 4. Effect of annealing duration and heating rate on XRD patterns collected in samples annealed at 1273 K. No major changes can be observed, which indicates that these two parameters have little effect on the mineralogy of the dust analogue.

of forsterite below T_g is confirmed for at least five different classes of amorphous materials, though this was never noticed so far. At $T_g \pm 20$ K forsterite is shown dominant in many of the annealed materials, but some studies report the formation of enstatite only. As discussed below, this may be caused by slight variations of cation dynamics as a function of the structure of the starting material. Finally, well above the glass transition, enstatite is strongly dominant. Forsterite is occasionally formed, but is always a minor component. This compilation of data emphasizes that our results do not strongly depend on the nature of the analogue but rather on the intrinsic properties of cation-oxygen bonds in silicates and oxides. Our results also point out that protoenstatite, the high-temperature polymorph of enstatite, can be quenched when grains are submicron-sized. Our Raman data together with those from Reynard et al. (2008) indicate that a spectral signature of this phase is present in the low-frequency region (Fig. 3). If so, Pen should be an extremely sensitive probe for fast thermal events in disks, such as lightening and shock waves, because the occurrence of these signatures would unambiguously indicate quasi-instantaneous cooling of the dust. On the other hand, the proportions of clino- and orthoenstatite may be more difficult to interpret in protoplanetary disks. The phase transition is not fast enough to accurately record and preserve information on thermal events or peak temperatures. The relative proportions may thus be the intermingled consequence of the heating rate, the cooling rates, the annealing duration, and the peak temperature.

We recently proposed a microscopic mechanism to explain the formation of forsterite from an amorphous precursor of an enstatite composition at a large degree of supercooling (Roskosz et al. 2009). The controlling parameter was shown to be the short lifetime of Mg-O bonds relative to Si-O bonds around the glass transition (several orders of magnitude of difference), which in turn favours the structural ordering of crystalline structures enriched in magnesium. Our experimental results are also consistent with those concerning calcium and aluminium-rich silicate glasses (see Roskosz et al. 2005, 2006). The mechanism can therefore be extrapolated to other alkali- and alkaline-rich materials, including those found in astrophysical environments. In the present study, the mineralogical transition occurs about 20 K below the nominal glass transition temperature determined on a quenched glass. This discrepancy is small, yet probably real. It may be caused by the structural differences between a glass and an amorphous material prepared by sol-gel. No accurate information is available on the dynamics of cations in sol-gel precursors. However, the fluffy structure of these materials and the surface diffusion that is faster in nanoporous materials than bulk diffusion is likely responsible for this small discrepancy. Because the glass transition temperature is the temperature below which diffusive processes involving the silicate network become extremely slow, one can anticipate that this characteristic temperature is shifted to lower temperatures in sol-gels and any other nanostructured and highly disordered material such as condensates and smokes. In other words, this temperature shift may represent the deviation of the behaviour of dust analogues of astrophysical relevance from the well-characterized behaviour of bulk, dense silicate glasses.

A similar interpretation may hold for the discrepancy observed between data reported by Jäger et al. (2003) and others (including ours). As noted by Jäger et al. (2003), their sol-gel materials contained significant amount of OH groups that were probably linked to the silica network (up to 1.3%). In silicate glasses and melts, hydroxyls have the same structural role as alkali and alkaline-earth cations. They induce a significant decrease of the glass transition temperature. Typically, in analogues of natural magmas (basalts, rhyolites, granites), the addition of such an amount of water to an anhydrous melt results in a decrease of T_g by 200−300 K (Richet et al. 1996; Dingwell et al. 1996). Based on these data, one can estimate the T_g of the starting material used by Jäger et al. (2003) to be close to 740 K (1040−300). This considerable decrease of T_g, over which diffusion decoupling rapidly becomes negligible can account for the fact that Jäger et al. (2003) only observed enstatite where others found forsterite. The effect of OH groups on the crystallization behaviour, already discussed by Jäger et al. (2003), can then be taken into account within our model. Furthermore, it calls for a detailed physical determination of the glass transition temperatures of cosmic dust analogues by conventional methods (Raman

Table 2. Compilation of reported mineralogical assemblages recovered after annealing of different amorphous starting materials of $MgSiO_3$ composition.

Temperature (K)	Starting Material	Mineralogy[a]	Analytical Methods[b]	References
Below T_g				
723–873	Sol-Gel (OH detected)	En	IR	1
933	Sol-Gel (precipitation)	Fo	XRD/IR	2
970	Sol-Gel (precipitation)	Fo	XRD/IR	2
973	Sol-Gel (xerogel)	Fo	XRD/TEM/SEM/IR	3
996	Glass powder (5–10 μm)	Fo+Trid	TEM/SEM/IR/XRD	4
1000	Laser ablation spherules	Fo+Trid	TEM	4
1000	Smokes	Fo	IR	5
1000	Sol-Gel (precipitation)	Fo	XRD/IR	2
$T_g \pm 20$ *K*				
1023	Sol-Gel (xerogel)	Fo+En	XRD/IR/SEM	6
1030	Glass powder (5–10 μm)	Oen	TEM	4
1033	Glass powder (5–10 μm)	Fo+Cen+Oen	XRD/TEM	3
1053	Sol-Gel (xerogel)	Fo+ En	XRD/IR/SEM	6
1060	Glass powder (5–10 μm)	Oen	TEM	4
1063	Sol-Gel (xerogel)	Fo+En	XRD/IR	6
Above T_g				
1073	Laser ablation spherules	En	SEM/IR	7
1073	Sol-Gel (xerogel)	Fo+En	XRD/IR	6
1080	Glass chips (100–130 μm)	Oen	IR/TEM/SEM/XRD	4
1080	Glass powder (5–10 μm)	Oen	TEM	4
1109	Sol-Gel (spray-drying)	Fo+Cen+Oen	XRD/DSC	8
1121	Glass chips (100–130 μm)	Oen	IR/TEM/SEM/XRD	4
1121	Glass powder (5–10 μm)	Oen	TEM	4
1165	Glass chips (100–130 μm)	Oen	IR/TEM	4
1173	Geopolymers	Fo + Oen	XRD/DTA	9
1173	Sol-Gel (precipitation)	Cen+Oen	XRD/DSC	8
1200	Smoke	Fo+Silica	IR	5
1273	Sol-Gel (xerogel)	Fo+Cen+Oen+Silica	XRD/TEM	3
1273	Laser ablation spherules	En	SEM/IR	7
1273	Sol-Gel (xerogel)	Cen+Oen	XRD/DTA	10

References. (1) Jäger et al. (2003); (2) Thompson et al. (2002); (3) Roskosz et al. (2009); (4) Fabian et al. (2000); (5) Hallenbeck & Nuth (1998); (6) Murata et al. (2009); (7) Brucato et al. (1999); (8) Douy (2002); (9) Van Long (2008); (10) Maliavski et al. (1997).

Notes. [(a)] Fo: forsterite; Trid: tridymite; En: enstatite (no distinctions between polymorphs); Oen: orthoenstatite; Cen: clinoenstatite; Cr: cristobalite.
[(b)] XRD: X-ray diffraction; IR: infra-red spectroscopy; TEM: transmission electron microscopy; SEM: scanning electron microscopy; DSC: differential scanning calorimetry; DTA: differential thermal analysis.

spectroscopy or differential scanning calorimetry) in order to make our model more predictive.

4.2. Thermal annealing around T_g as one of the processes responsible for the mineralogical zoning of protoplanetary disks

The sharp change of mineralogy observed through the glass transition domain may explain recent VLTI and *Spitzer* observations and helps to understand thermal processing of dust in protoplanetary disks. First, from VLTI MIDI observations, Van Boekel et al. (2004) showed that crystalline materials are more abundant in the very inner part of disks than in the more outer part. Despite this result, no obvious correlation has been found between stellar/disk parameters or age of the systems and the crystallinity of the dust (Henning 2010). This may be owing to additional processes such as irradiation in the disk (Glauser et al. 2009) or to episodic heating events such as the eruption of the young Sun-like star EX Lupi recently reported by Abrahám et al. (2009). Data from Van Boekel et al. (2004) also indicate that olivine is more abundant close to the protostar while pyroxenes dominate the mineralogy at farther distances. This mineralogical zoning can be simply explained by evaporation-condensation mechanisms in hot regions close to the star that promotes the formation of olivines at higher temperature than pyroxene. Associated to mixing models, this process was also, to some extent, supported by the high crystallinity and the mineralogy of cometary materials collected during the Stardust mission (Zolensky et al. 2006). However, studies of disks around T Tauri and Herbig Ae stars by *Spitzer* reveal a change in the relative proportions of the different species of crystalline silicates with radial distance (Bouwman et al. 2008; Meeus et al. 2009; Sargent et al. 2009b; Watson et al. 2009; Juhàsz et al. 2010). The *Spitzer* orbiter probed more distant regions of the disk (from 1 AU to 15 AU) than the VLTI MIDI and found that enstatite is dominant in the inner region, while forsterite dominates in colder outer regions. Moreover, silica polymorphs such as cristobalite, tridymite and quartz are also detected (Sargent et al. 2009a). These two observations are major caveats for a straightforward model involving equilibrium evaporation-condensation mechanism associated to a certain degree of radial mixing (e.g. Gail 2004). Contrary to the subsolidus crystallization pathway described in this study (i.e. a crystallization occuring at low temperature and in the absence of any molten phase), this mechanism cannot account for the mineralogical trend forsterite-enstatite-forsterite+SiO_2 polymorphs.

Amorphous cosmic silicate dust can be modelled as magnesiosilicates with compositions lying between $MgSiO_3$ and Mg_2SiO_4 (named enstatite and forsterite components in the following). The annealing of the olivine component likely produces olivine crystals because this phase is known to form easily and is the most Mg-rich crystalline silicate. As a consequence, a subsolidus pathway should not affect its formation. However, based on solar abundances of the elements (Molster et al. 1999), the relative proportion of the olivine component must be low (less than 50%) compared to the total amount of the amorphous silicate dust. It is therefore difficult to understand why crystalline olivine is dominant in regions where evaporation-condensation is not at work. Our data suggest that annealing of the second dust component (enstatite) also forms olivine when the temperature is below ~1000 K. In this condition, the annealing of the silicate dust directly leads to a mineralogy dominated by olivine. Conversely, annealing of the enstatite component in warmer, inner regions would result essentially in the formation of crystalline enstatite, which mixed with the crystalline olivine formed from the amorphous olivine precursor would still give a mineralogy dominated by enstatite. The crystallization transition around T_g explains the enstatite-forsterite zoning revealed by *Spitzer*. Moreover, it explains the occurrence of silica crystalline and amorphous polymorphs in relatively cold zones of the disk. It is the consequence of crystallizing forsterite from an amorphous $MgSiO_3$ precursor, which led to some SiO_2 as by-product (amorphous in a first step). The kinetics of crystallization of silica below 1200 K cannot be studied in a laboratory. The timescale of silica crystallization is thus unclear, but if time and temperature are sufficient, the crystallization scheme identified in this study provides the pathway to form the SiO_2 amorphous precursor. It may then be proposed that the amount of silica should be commensurate with the amount of forsterite produced from the enstatite component. If 10% of olivine is produced, then, ultimately, after the complete crystallization of the dust, one should obtain 10% of crystalline silica. In this respect, the metastable mineralogical assemblages of olivine and silica that have recently been found in Stardust samples (Leroux et al. 2010; Mikouchi et al. 2007) confirm this close association which was initially proposed by Sargent et al. (2009a) on spectroscopic bases. A subsolidus crystallization pathway must then be combined to evaporation-condensation mechanisms at work in the innermost regions to fully capture the processes at the origin of the mineralogical zoning of disks.

5. Conclusion

Experimental annealing of silicate dust analogues were conducted in various conditions to determine the temperature dependence of the mineralogy of protoplanetary disks. Below 1000 K, forsterite is clearly the main crystalline phase produced even from a starting material of enstatite composition and may easily be associated to silica polymorphs. A sharp change of this mineralogy is found at 1000 K; above, pyroxenes become the dominant phase. Within this class of minerals, the different polymorphs are produced in various proportions as the annealing conditions vary. However, only the high-temperature polymorph (protoenstatite) seems to record very specific conditions and could therefore be used as an excellent proxy for fast high-temperature processes occurring in disks. The transition orthoclinoenstatite may be more difficult to interpret in details. All our data suggest that the subsolidus crystallization pathway has a strong influence on the mineralogical zoning observed in disks. Associated to evaporation/condensation processes at work in the inner part of disks, it can explain the zoning olivine-pyroxene-olivine+silica recently documented by the *Spitzer* observations.

Acknowledgements. The preliminary version of this article benefited from the thorough and constructive comments by an anonymous referee. We thank M. Moreau for the help and expertise provided during Raman work at the LASIR (University of Lille 1). B. Reynard is thanked for fruitful discussions and for his help during the identification of protoenstatite by Raman spectroscopy. The "Fonds Européen de Développement Régional (FEDER)", "CNRS", "Région Nord Pas-de-Calais" and "Ministère de l'Education Nationale de l'Enseignement Supérieur et de la Recherche" are acknowledged for fundings of X-ray diffractometers. This work was granted by the PNP Program of the French CNRS-INSU.

References

Abrahám, P., Juhàsz, A., Dullemond, C., Kòspàl, A., & van Boekel, R. 2009, Nature, 459, 224
Bouwman, J., Meeus, G., de Koter, A., et al. 2001, A&A, 375, 950
Bouwman, J., Henning, T., Hillenbrand, L., Meyer, M., & Pascussi, I. 2008, ApJ, 683, 479
Brucato, J. R., Colangeli, L., Mennella, V., Palumbo, P., & Bussoletti, E. 1999, A&A, 348, 1012
Davoisne, C., Djouadi, Z., d'Hendecourt, L., Jones, A., & Deboffle, D. 2006, A&A, 448, L1
Dingwell, D., Romano, C., & Hess, K. 1996, Contributions to Mineralogy and Petrology, 124, 19
Douy, A. 2002, Journal of Sol-Gel Science and Technology, 24, 221
Fabian, D., Jäger, C., Henning, J., Dorshner, J., & Mutschke, H. 2000, A&A, 364, 282
Gail, H.-P. 2004, A&A, 413, 571
Glauser, A., Güdel, M., Watson, D., Henning, T., & Schegerer, A. 2009, A&A, 508, 247
Gruener, G., Odier, P., De Sousa Meneses, D., Florian, P., & Richet, P. 2001, Phys. Rev. B, 64, 24206
Hallenbeck, S. L., & Nuth, J. A. 1998, Icarus, 131, 198
Henning, T. 2010, Ann. Rev. Astron. Astrophys., 48, 21
Henning, T., & Stognienko, R. 1996, A&A, 311, 291
Jäger, C., Dorshner, J., Mutschke, H., Posch, T., & Henning, T. 2003, A&A, 408, 193
Juhàsz, A., Bouwman, J., Henning, T., Acke, B., & van den Ancker, M. 2010, ApJ, 721, 431
Leroux, H., Kearsley, A. T., & Troadec, D. 2010, Lunar and Planetary Institute Conference Abstracts, 1621
Maliavski, N. I., Dushkin, O. V., Tchekounova, E. V., Markina, J. V., & Scarinci, G. 1997, Journal of Sol-Gel Science and Technology, 8, 571
Meeus, G., Juhàsz, A., Henning, T., Bouwman, J., & Chen, C. 2009, A&A, 497, 479
Mikouchi, T., Tachikawa, O., Hagiya, K., et al. 2007, Lunar and Planetary Institute Conference Abstracts, 1338
Min, M., Waters, L., de Koter, A., et al. 2007, A&A, 462, 789
Molster, F., Yamamura, I., Waters, L., et al. 1999, Nature, 401, 563
Molster, F. J., Waters, L. B. F. M., Tielens, A. G. G. M., Koike, C., & Chihara, H. 2002, A&A, 382, 241
Murata, K., Chihara, H., Koike, C., et al. 2009, ApJ, 697, 836
Pollack, J., Hollenbach, D., Beckwith, S., et al. 1994, ApJ, 421, 615
Reynard, B., Bass, J. D., & Jackson, J. M. 2008, J. Eur. Ceram. Soc., 28, 2459
Richet, P., Lejeune, A. M., Holtz, F., & Roux, J. 1996, Chemical Geology, 128, 185
Rietmeijer, F. J. M., Hallenbeck, S. L., Nuth, J. A., & Karner, J. M. 2002, Icarus, 156, 269
Roskosz, M., Toplis, M. J., Besson, P., & Richet, P. 2005, Journal of Non-Crystalline Solids, 351, 1266
Roskosz, M., Toplis, M. J., & Richet, P. 2006, Journal of Non-Crystalline Solids, 352, 180
Roskosz, M., Gillot, J., Capet, F., Roussel, P., & Leroux, H. 2009, ApJ, 707, L174
Sargent, B. A., Forrest, W. J., Tayrien, C., et al. 2009a, ApJ, 690, 1193
Sargent, B. A., Forrest, W. J., Tayrien, C., et al. 2009b, ApJS, 182, 477
Smyth, J. R. 1974, Am. Mineral., 59, 345
Thompson, S. P., Fonti, S., Verrienti, C., et al. 2002, A&A, 395, 705
Thompson, S. P., Fonti, S., Verrienti, C., et al. 2003, Meteorit. Planet. Sci., 38, 457
Van Boekel, R., Min, M., Leinert, C., et al. 2004, Nature, 432, 479
Van Long, T. 2008, Ceram. Internat., 34, 1763
Watson, D. M., Leisenring, J. M., Furlan, E., et al. 2009, ApJ, 180, 84
Zolensky, M. E., Zega, T. J., Yano, H., et al. 2006, Science, 314, 1735